



CHORUS

This is the accepted manuscript made available via CHORUS. The article has been published as:

Ratios of double to single ionization of He and Ne by strong 400-nm laser pulses using the quantitative rescattering theory

Zhangjin Chen, Xiaojin Li, Oleg Zatsarinny, Klaus Bartschat, and C. D. Lin

Phys. Rev. A **97**, 013425 — Published 29 January 2018

DOI: [10.1103/PhysRevA.97.013425](https://doi.org/10.1103/PhysRevA.97.013425)

Ratios of double to single ionization of He and Ne by strong 400 nm laser pulses using the quantitative rescattering theory

Zhangjin Chen and Xiaojin Li

*Department of Physics, College of Science, Shantou University,
Shantou, Guangdong 515063, People's Republic of China*

Oleg Zatsarinny and Klaus Bartschat

Department of Physics and Astronomy, Drake University, Des Moines, Iowa 50311, USA

C. D. Lin

*J. R. Macdonald Laboratory, Physics Department,
Kansas State University, Manhattan, Kansas 66506-2604, USA*

(Dated: January 16, 2018)

We present numerical simulations of the ratio between double and single ionization of He and Ne by intense laser pulses at wavelengths of 390 nm and 400 nm, respectively. The yields of doubly charged ions due to nonsequential double ionization (NSDI) are obtained by employing the quantitative rescattering (QRS) model. In this model, the NSDI ionization probability is expressed as a product of the returning electron wave packet (RWP) and the total scattering cross sections for laser-free electron impact excitation and electron impact ionization of the parent ion. According to the QRS theory, the same RWP is also responsible for the emission of high-energy above-threshold ionization (HATI) photoelectrons. To obtain absolute double-ionization yields, the RWP is generated by solving the time-dependent Schrödinger equation (TDSE) within a one-electron model. The same TDSE results can also be taken to obtain single-ionization yields. By using the TDSE results to calibrate single ionization and the RWP obtained from the strong-field approximation, we further simplify the calculation such that the nonuniform laser intensity distribution in the focused laser beam can be accounted for. In addition, laser-free electron impact excitation and ionization cross sections are calculated using the state-of-the-art many-electron R -matrix theory. The simulation results for double to single ionization ratios are found to compare well with experimental data and support the validity of the nonsequential double ionization mechanism for the covered intensity region.

PACS numbers: 32.80.Fb, 32.80.Rm, 34.50.Rk, 34.80.Dp

I. INTRODUCTION

The classical three-step rescattering model [1, 2] has been widely employed to qualitatively interpret laser-induced rescattering processes in the past two and a half decades. According to this model, an electron is first ionized near the peak of the laser's oscillating electric field. In the second step, the electron is subsequently driven by the laser field and has the chance to return back to the parent ion when the field changes direction. Upon return (third step) the electron may scatter from the ion core. The elastic scattering can result in high-order above-threshold ionization (HATI) [3] photoelectrons. The returning electron can also recombine with the parent ion with the emission of photons for high-order harmonics generation (HHG) [4]. Both HATI and HHG are basically one-electron processes and can approximately be treated by using a single-electron model. For multielectron targets, the returning electron may ionize another electron of the ion, or it may excite the electron to an excited state, which is subsequently ionized by the laser. These latter processes result in nonsequential double ionization (NSDI) [5, 6]. While HATI and HHG may be calculated accurately within a single-electron model by solving the

time-dependent Schrödinger equation (TDSE), NSDI is intrinsically a two-electron process resulting in two continuum electrons in the final state. Accurate calculations of NSDI, therefore, continue to present a great challenge, for which sophisticated theoretical modeling beyond the single-active electron (SAE) approximation is needed.

According to the three-step model, HATI, HHG, and NSDI all result from electron recollisions with the parent ion. Nevertheless, the three-step model was incapable of making actual calculations before the quantitative rescattering (QRS) model [7] was developed. According to the QRS model, the yields for HATI, NSDI, and HHG can be expressed as a product of the returning electron wave packet (RWP) with various field-free electron-ion scattering cross sections, namely elastic electron scattering, electron impact ionization, and photo-recombination, respectively.

While the QRS model developed by Lin and coworkers has been widely used to simulate photoelectron energy spectra and two-dimensional momentum distributions for both HATI electrons [8–11] and HHG spectra [12, 13] with great success, there have been fewer investigations of NSDI. To study NSDI, field-free inelastic electron impact excitation cross sections and electron impact ionization cross sections are needed over a broad energy range.

Thus, while a few NSDI studies have been carried out with the QRS model, such as the laser-intensity dependence of nonsequential double ionization [14, 15] as well as the correlated electron momentum distributions and their dependence on the carrier-envelope phase [16, 17], the accuracy is always marred by the limited quality of the field-free inelastic electron impact excitation and ionization cross sections. Such limitations may not be too severe for studying the laser-intensity dependence and the CEP-dependence of the NSDI process, but this implies that the role of target structure has not been clearly explored in these experiments.

From the experimental point of view, the ratios of double ionization versus single ionization by a strong laser field vs. laser intensity are likely the most accurate parameters that can be determined in the laboratory. They can be determined by taking the ratio of doubly to singly charged ions. While the actual experimental intensity cannot be accurately determined in general, a method based on the PPT (Perelomov-Popov-Terent'ev) theory [18] was suggested recently to retrieve accurate peak laser intensity from the measured ionization signals efficiently [19]. The total single-ionization probability can also be accurately calculated by solving the TDSE within the SAE model for short pulses. If there is a reliable method to calculate the NSDI yields, then the theoretical ratios can be compared to the experimental ratios. In such comparisons, both single- and double-ionization calculations should account for the actual intensity distributions within a focused laser beam.

While single-ionization yields can be calculated for a known laser field with reasonable accuracy, this is not the case for double ionization, especially for the NSDI process. A direct numerical solution of the TDSE for the NSDI process for the two-electron helium atom in an 800 nm field has still not yet been reported due to the difficulties of achieving numerical convergence. However, the ratio for a 390 nm laser pulse was predicted by Parker *et al.* [20]. Since NSDI is a rescattering process, it is interesting to investigate whether accurate total NSDI yields can be determined using the QRS theory. In the present paper, this is carried out with two recent developments. First, the returning electron wave packet in the QRS is properly normalized to the TDSE results. Second, accurate electron impact excitation and ionization cross sections for He⁺ and Ne⁺ in the low-energy region are calculated using the many-electron *B*-spline *R*-matrix (BSR) method [21, 22]. In order to compare with the ratios obtained from actual experiments, the calculations were carried out for He exposed to a 390 nm laser pulse and Ne exposed to a 400 nm laser pulse.

The remainder of the present paper is arranged as follows. Section II summarizes the ingredients of the theoretical methods. The details of the numerical procedure and the final simulated results are presented in Sec. III. Finally, our conclusions are given in Sec. IV. Unless indicated otherwise, atomic units (a.u.) ($\hbar = |e| = m = 4\pi\epsilon_0 = 1$) are used throughout the manuscript.

II. THEORETICAL MODEL

A. The strong-field approximation

In the familiar strong-field approximation (SFA), the first two terms of the perturbation series, called SFA1 and SFA2, respectively, express the momentum-dependent ionization amplitude as

$$f_{\text{SFA}}(\mathbf{p}) = f_{\text{SFA1}}(\mathbf{p}) + f_{\text{SFA2}}(\mathbf{p}), \quad (1)$$

where \mathbf{p} is the momentum of the detected photoelectron.

The SFA1 amplitude is given by

$$f_{\text{SFA1}}(\mathbf{p}) = -i \int_{-\infty}^{\infty} dt \langle \chi_{\mathbf{p}}(t) | \mathbf{r} \cdot \mathbf{E}(t) | \beta(t) \Psi_i(t) \rangle, \quad (2)$$

where $\mathbf{E}(t) = -\partial\mathbf{A}(t)/\partial t$ is the electric field of the laser, and Ψ_i is the initial ground-state wave function. The decay factor $\beta(t)$ introduced in Eq. (2) accounts for the depletion of the initial state, which is given by

$$\beta(t) = \exp \left[- \int_{-\infty}^t dt' W(t')/2 \right], \quad (3)$$

where $W(t)$ is the time-dependent modified ADK (Ammosov-Delone-Krainov) [23] rate proposed by Tong and Lin [24]. The Volkov state $\chi_{\mathbf{p}}$ in Eq. (2) is given by

$$\langle \mathbf{r} | \chi_{\mathbf{p}}(t) \rangle = \frac{1}{(2\pi)^{3/2}} e^{i[\mathbf{p} + \mathbf{A}(t)] \cdot \mathbf{r}} e^{-iS(\mathbf{p}, t)}, \quad (4)$$

where the action S is

$$S(\mathbf{p}, t) = \frac{1}{2} \int_{-\infty}^t dt' [\mathbf{p} + \mathbf{A}(t')]^2. \quad (5)$$

The second term in Eq. (1) accounts for laser-induced rescattering, i.e., elastic scattering of the returning electron from the parent ion. This term, called SFA2, is expressed as

$$f_{\text{SFA2}}(\mathbf{p}) = - \int_{-\infty}^{\infty} dt \int_t^{\infty} dt' \int d\mathbf{k} \langle \chi_{\mathbf{p}}(t') | V | \chi_{\mathbf{k}}(t') \rangle \times \langle \chi_{\mathbf{k}}(t) | H_i(t) | \beta(t) \Psi_i(t) \rangle, \quad (6)$$

where V is the scattering potential. It takes the form

$$V(\mathbf{r}) = -\frac{Z_{\text{eff}}}{r} e^{-\alpha r}, \quad (7)$$

where α is a screening factor introduced to avoid the singularity in the integrand in Eq. (6). The SFA2 amplitude (6) consists of a five-dimensional integration, which can be reduced to two dimensions by using the saddle-point approximation for the integration with respect to \mathbf{k} , as proposed by Lewenstein *et al.* [25].

With the momentum-dependent ionization amplitude, the momentum distribution of an electron emitted with energy $E = p^2/2$ in the direction of $\hat{\mathbf{p}}$ is given by

$$\frac{d^3 \mathcal{P}_{\text{SFA}}^+}{d^3 p} = |f_{\text{SFA}}(\mathbf{p})|^2. \quad (8)$$

From Eq. (8), we obtain the energy spectra

$$\frac{d\mathcal{P}_{\text{SFA}}^+}{dE} = 2\pi\sqrt{2E} \int_{-1}^1 |f_{\text{SFA}}(\mathbf{p})|^2 d(\cos\theta), \quad (9)$$

and the total ionization probability for single ionization

$$\mathcal{P}_{\text{SFA}}^+ = \int \frac{d\mathcal{P}_{\text{SFA1}}^+}{dE} dE. \quad (10)$$

In Eq. (10), the contribution from SFA2 is neglected since it is much smaller than the SFA1.

B. The time dependent Schrödinger equation

The numerical solution of the Schrödinger equation in a time-dependent laser field provides a reliable quantum description of both direct ionization and HATI due to elastic rescattering. Within the SAE approximation, the TDSE for an atom in the presence of a linearly polarized laser field, in the length gauge, can be written as

$$i\frac{\partial}{\partial t}\Psi(\mathbf{r}, t) = \left[-\frac{1}{2}\nabla^2 + V_{\text{SAE}}(r) + \mathbf{r} \cdot \mathbf{E}(t) \right] \Psi(\mathbf{r}, t), \quad (11)$$

where the model potential V_{SAE} for atoms is parameterized in the form

$$V_{\text{SAE}}(r) = -\frac{1 + a_1 e^{-a_2 r} + a_3 r e^{-a_4 r} + a_5 e^{-a_6 r}}{r}. \quad (12)$$

The parameters in Eq. (12) are obtained by fitting the calculated binding energies from this potential to the experimental binding energies of the ground state and the first few excited states of the target atom [26].

The time-dependent equation is solved by using a second-order split operator method [27, 28], and the wave function is expanded into direct products of discrete-variable-representation basis sets [29–31] associated with Legendre polynomials.

The momentum-dependent ionization amplitude is obtained by projecting the total final wave function at the end of the laser pulse onto eigenstates of a continuum electron with momentum \mathbf{p} ,

$$f_{\text{TDSE}}(\mathbf{p}) = \langle \Phi_{\mathbf{p}}^- | \Psi(t = \infty) \rangle, \quad (13)$$

where the continuum state $\Phi_{\mathbf{p}}^-$ is obtained by solving the differential equation

$$\left[-\frac{1}{2}\nabla^2 + V_{\text{SAE}}(r) \right] \Phi_{\mathbf{p}}^- = \frac{p^2}{2} \Phi_{\mathbf{p}}^-. \quad (14)$$

C. The QRS model for HATI

According to the QRS model, the momentum distribution for HATI photoelectrons can be expressed as a product of the returning electron wave packet and the

elastic differential cross section (DCS) for free electrons scattering from the target ion. In the SFA model, the direct ionization and the ionization due to rescattering are calculated by SFA1 and SFA2 separately, and only SFA2 accounts for rescattering. Therefore, for a photoelectron with momentum \mathbf{p} detected at an angle θ with respect to the polarization vector of the laser field, we have

$$|f_{\text{SFA2}}(\mathbf{p})|^2 = W_{\text{SFA2}}(k_r) \frac{d\sigma_B(k_r, \theta_r)}{d\Omega_r}, \quad (15)$$

where $W_{\text{SFA2}}(k_r)$ is the RWP describing the momentum distribution of the returning electron. Furthermore, $d\sigma_B(k_r, \theta_r)/d\Omega_r$ is the DCS obtained in the first-order Coulomb-Born or plane-wave Born approximation (PWBA) for elastic scattering of the returning electron from the parent ion with momentum k_r at an angle θ_r with respect to the direction of the returning electron. In the PWBA, where the continuum electron wave functions are represented by plane waves, the elastic scattering amplitude is given by

$$f(\mathbf{q}) = -\frac{1}{2\pi} \int \exp(i\mathbf{q} \cdot \mathbf{r}) V(r) d\mathbf{r} = -\frac{2Z_{\text{eff}}}{q^2 + \alpha^2}, \quad (16)$$

where \mathbf{q} is the momentum transfer. The latter is related to the rescattering angle θ_r and the returning electron momentum k_r by

$$q = 2k_r \sin(\theta_r/2). \quad (17)$$

Consequently, the elastic scattering DCS in Eq. (15) can be expressed as

$$\frac{d\sigma_B(k_r, \theta_r)}{d\Omega_r} = |f(\mathbf{q})|^2. \quad (18)$$

The photoelectron momentum \mathbf{p} and the momentum \mathbf{k}_r of the returning electron after scattering are related by

$$\mathbf{p} = \mathbf{k}_r - \mathbf{A}_r, \quad (19)$$

where \mathbf{A}_r is the instantaneous vector potential at the time when the electron returns to the origin. Furthermore, to establish a one-to-one relation between \mathbf{p} and \mathbf{k}_r , one may use, approximately,

$$k_r \approx 1.26|A_r| \quad (20)$$

for returning electrons near the cutoff. This may be calculated from the one-dimensional classical theory of a free electron in an oscillating laser field [8]. Similarly, for the TDSE calculations, the momentum distribution for HATI photoelectron can be expressed as

$$|f_{\text{TDSE}}(\mathbf{p})|^2 = W_{\text{TDSE}}(k_r) \frac{d\sigma(k_r, \theta_r)}{d\Omega_r}. \quad (21)$$

It has been carefully verified that, in the above equation, if $W_{\text{TDSE}}(k_r)$ is replaced by $W_{\text{SFA2}}(k_r)$ obtained from Eq. (15) and $d\sigma(k_r, \theta_r)/d\Omega_r$ is evaluated using standard

potential scattering theory, the shapes of the TDSE momentum distributions for HATI electrons are well reproduced [8], while the absolute magnitudes are different by a constant factor. On the other hand, with the TDSE momentum distributions and accurate DCSs, $W_{\text{TDSE}}(k_r)$ obtained from Eq. (21) is also in good agreement with $W_{\text{SFA2}}(k_r)$, except for a normalization factor owing to the error of ionization rate in the SFA model.

D. The QRS model for NSDI

The QRS model can be applied to all laser-induced rescattering processes. Unlike for HATI electrons, where the returning electrons are elastically scattered by the ion, in NSDI the returning electrons are inelastically scattered by impact ionization and excitation processes. The total NSDI yield can be calculated from [14, 15]

$$\mathcal{P}^{2+} = \int dE_r [W_L(E_r) + W_R(E_r)] \times [\sigma_{\text{exc}}(E_r) + \sigma_{e2e}(E_r)], \quad (22)$$

where $\sigma_{\text{exc}}(E_r)$ and $\sigma_{e2e}(E_r)$ are the total cross sections (TCSs) for electron impact excitation and ionization from the ground state of the target ion at incident energy E_r . This is related to the momentum of the returning electron by $E_r = k_r^2/2$, and $W_L(E_r)$ and $W_R(E_r)$ are the RWP extracted from the “left” ($p_z < 0$) and the “right” ($p_z > 0$) sides of the momentum distributions for HATI photoelectrons, respectively. For long pulses considered here, $W_L(E_r) = W_R(E_r)$. As mentioned above, it has been demonstrated that the RWP obtained from SFA2 and the TDSE agree well with each other [8], except for an overall normalization factor.

Clearly, it is much more convenient to employ SFA2 rather than TDSE to calculate the RWP, especially in the case of long laser pulses at high intensities, for which the TDSE calculations are extremely challenging. Consequently, all the RWP in Eq. (22) are taken from the SFA2 calculations after the normalization factor was determined by comparing the RWPs with those from a few representative TDSE calculations.

It should be noted that, in Eq. (22), we assumed that all excited electrons are tunnel-ionized. The integration should be performed over all energies higher than the threshold energy of the returning electron.

E. Lowering of the threshold potential

According to the rescattering model, the maximum kinetic energy that a returning electron can gain from the field is $3.17 U_p$, where U_p is the electron ponderomotive energy, which is proportional to the intensity. Since a minimum kinetic energy is required for the returning electron to ionize an electron of the residual ion or to promote this electron to an excited state, a single threshold

energy of the ion is always predicted by the QRS model. This model, however, as pointed out by van der Hart and Burnett [32], does not account for the effect of the laser field on the target ion. In particular, one expects that the laser field will lower the threshold energy of the returning electron for excitation and ionization, as depicted in Fig. 1 in the static limit. The amount of lowering can be calculated from the saddle point of

$$V(z) = zF_r - Z/z. \quad (23)$$

Here the reduction of the potential at the saddle is given by

$$V_b = -2\sqrt{Z|F_r|}, \quad (24)$$

where F_r is the electric field at the instant of scattering, and $Z = 2$ for electron impact ionization and $Z = 1$ for electron impact excitation of a singly charged ion, respectively. Thus, for electron impact ionization and excitation taking place in an electric field, the required minimum kinetic energies of the laser-induced returning electron are lowered by $|V_b|$ compared to the field-free case. In order to account for this effect, therefore, Eq. (22) should be modified as

$$\mathcal{P}^{2+} = \int dE_r [W_L(E_r) + W_R(E_r)] \times [\sigma_{\text{exc}}(E_r + 2\sqrt{|F_r|}) + \sigma_{e2e}(E_r + 2\sqrt{2|F_r|})]. \quad (25)$$

Since the lowering of the potential saddle changes with time, an effective average lowered potential at the return time of $t = 290^\circ/\omega$ was used in this correction, see Ref. [15]. Note that the lowered potential depends on the laser intensity.

In Ref. [32] it is suggested that for electron impact ionization, the minimum energy with which the ejected electron can escape is also lowered in the presence of the electric field, therefore another term corresponding to the barrier height should be added to the scattering energy. Like Eremina *et al.* [33] we do not follow their suggestion. In our *R*-matrix calculation, the modification of the potential cannot be separated into before and after the collision since energy is conserved in the (e , $2e$) collision.

F. Focal averaging

The procedures outlined above only apply to a single intensity. In an actual experiment, on the other hand, the intensity distribution of a focused laser beam is not uniform in space. Since the electrons collected experimentally originate from atoms located somewhere in the interaction volume, focal-volume averaging has to be taken into account in the numerical simulations when comparing to experiment. To achieve this, the total single ionization rate at a peak intensity I_0 is expressed as

$$\bar{\mathcal{P}}^+(I_0) = \int_0^{I_0} \mathcal{P}^+(I) \frac{\partial V}{\partial I} dI. \quad (26)$$

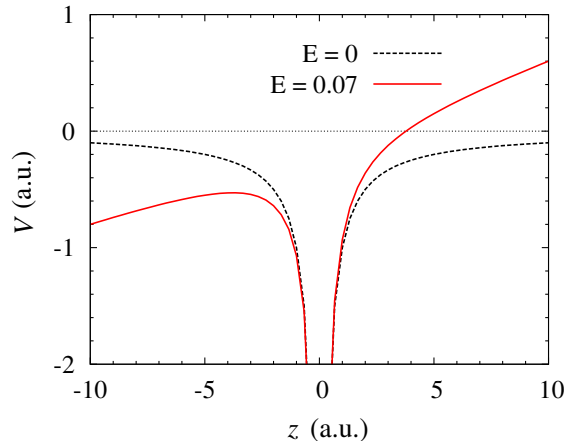


FIG. 1: Barrier in the combined atomic and electric field potential along the polarization axis z of the laser field (red solid curve). The atomic potential is chosen as Coulombic with $Z = 1$ (black dashed curve) and the (static) electric field is chosen as 0.07. The latter corresponds to the returning time for $\omega t = 290^\circ$ in a laser field with a peak intensity of 15×10^{14} W/cm 2 .

For a laser beam with a Lorentzian distribution in the propagation direction and a Gaussian distribution in the transverse direction, the focal volume in Eq. (26) is given by [28]

$$\frac{\partial V}{\partial I} \propto \frac{1}{I} \left(\frac{I_0}{I} + 2 \right) \sqrt{\frac{I_0}{I} - 1}. \quad (27)$$

To obtain total NSDI yield to compare with experiment, volume integration over Eq. (25) has to be carried out. Since the wave packet is a smooth function of returning electron energy, we can simplify the volume integration to

$$\bar{\mathcal{P}}^{2+} = \int dE_r [\bar{W}_L(E_r) + \bar{W}_R(E_r)] \times [\sigma_{\text{exc}}(E_r + 2\sqrt{|F_r|}) + \sigma_{e2e}(E_r + 2\sqrt{2|F_r|})], \quad (28)$$

where \bar{W}_L and \bar{W}_R are the focal-volume-averaged RWP. It has been tested that the difference between the double ionization yield obtained from Eq. (28) and that by performing focal volume integration on Eq. (25) directly is less 8%.

III. RESULTS AND DISCUSSION

We aim to simulate the experimentally measured double-to-single ionization ratios for He in 120 fs linearly polarized laser pulses at 390 nm [34], and Ne in 40 fs linearly polarized pulses at 400 nm [35]. For this purpose, we first evaluated the total single ionization rate using the SFA1. Figure 2 shows the simulated yields of Ne $^+$

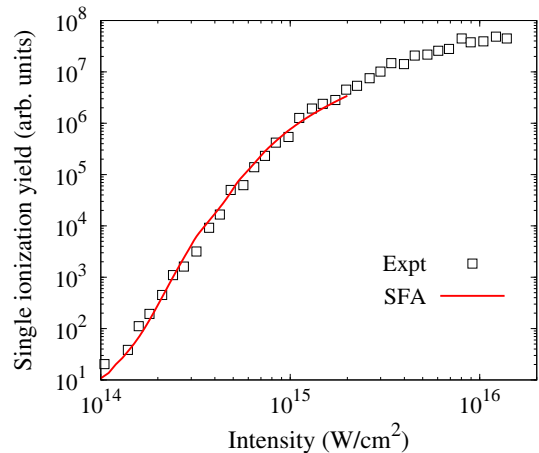


FIG. 2: Single-ionization yields for Ne exposed to linearly polarized laser pulses at 400 nm. The experimental data are taken from Ekanayake *et al.* [35], and the simulated results from the SFA model are normalized for good visual agreement with experiment. The calculations include the integration over the focal volume of the laser.

ions as a function of peak intensity together with the corresponding experimental data of Ekanayake *et al.* [35]. It can be seen that the normalized SFA1 results for Ne are in very good agreement with experiment over the entire intensity range considered here. Note that the integration over the focal volume of the laser was performed in the numerical simulations.

In order to obtain the double ionization yields for NSDI, we need to evaluate the RWP and the TCS for electron impact excitation and ionization of the target ions. The RWPs calculated using Eq. (15) with the focal volume effect considered are shown in Fig. 3 for He and Ne exposed to linearly polarized laser pulses at 390 nm and 400 nm, respectively. It has been shown that the RWP depends on the screening factor introduced in Eq. (7). If a large screening factor is used, however, the RWP converges [15]. In this paper, like Ref. [15], we chose a screening factor $\alpha = 4$. For the NSDI process, the returning electron energy is large, meaning that scattering is being contributed from small distance of the atom. Since the SFA2 integral contains fast oscillating exponent, choosing a large alpha avoids the need to integrate over a large volume which would incur numerical errors. The choice of large alpha is to avoid such errors in the wave packet included in Eq. (28). Since the wave packet calculated from SFA2 still has to be normalized to the one from TDSE at one energy point, the specific α used is not critical. Figure 3 shows that the RWPs at four selected intensities drop rapidly at low energies, followed by a plateau at high energies. Going into more detail, the flatness of the RWPs at high energies for He is slightly different from that seen for Ne. This is at least partially due to the fact that different laser parameters were used for these two atoms and that the focal-volume

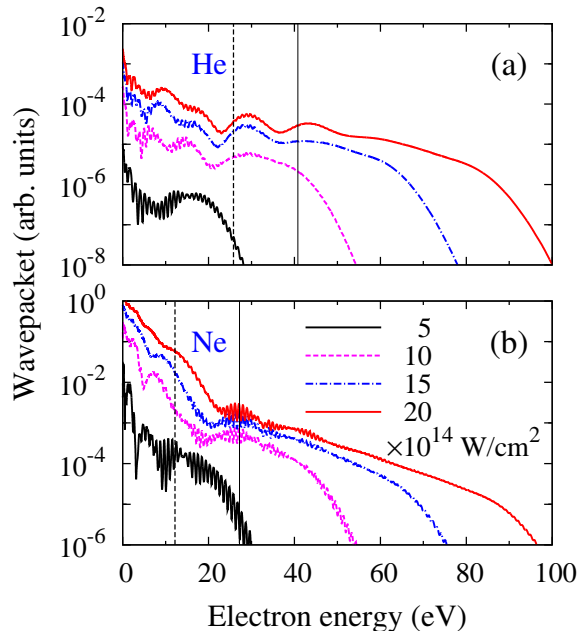


FIG. 3: Returning electron wave packets for (a) He and (b) Ne in linearly polarized laser pulses at 390 nm and 400 nm, respectively. The calculations include the integration over the focal volume of the laser. The vertical solid lines mark the excitation thresholds of He^+ and Ne^+ in the field-free case, while the vertical dotted lines mark the corresponding thresholds for excitations in the field at a peak intensity of $15 \times 10^{14} \text{ W/cm}^2$. See text for details.

integration was included.

In Fig. 3 the excitation thresholds of He^+ (40.8 eV) and Ne^+ (27.0 eV) in the field-free case are marked by the vertical solid lines, while the vertical dotted lines mark the corresponding thresholds for excitations in the field at a peak intensity of $15 \times 10^{14} \text{ W/cm}^2$ when the returning electron approaches the parent ion at the time $t = 290^\circ/\omega$. It should be emphasized that, as an assumption, the electric field at the moment of recollision does not affect the energies of any bound states. The change of threshold only means that the minimum energy required for the returning electron to promote the ground-state electron to the excited state is reduced due to the lower potential barrier caused by the electric field.

We use the BSR method [21, 22] to calculate the TCSs for ionization and excitation of He^+ and Ne^+ by electron impact. The results are plotted in Fig. 4. The details of the R -matrix calculations for electron impact ionization and excitation of He^+ were given in our previous paper [15], and the ideas for Ne^+ are similar. With a large number of pseudostates included in the close-coupling expansion, the numerical results obtained here can be considered converged to an overall accuracy of a few percent or even better. It should be noted that for laser-induced collisions of the returning electron with the parent ion, only singlet scattering occurs for both cases. This is due to the fact that the returning electron

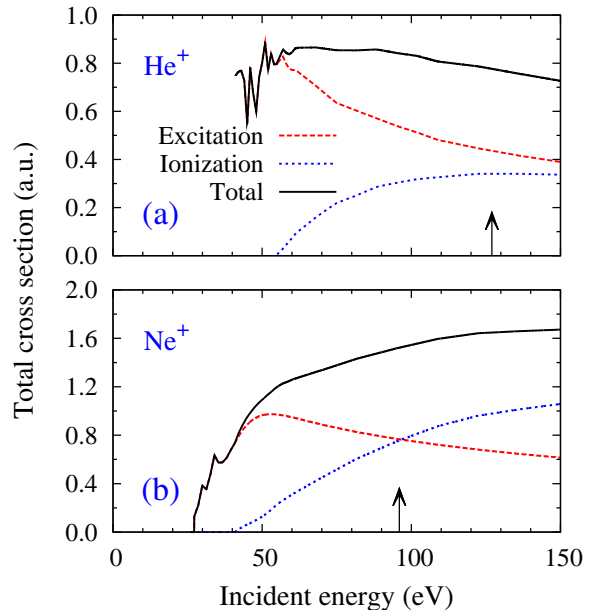


FIG. 4: Total cross sections for electron impact ionization (blue dotted curves) and excitation (red broken curves) of (a) He^+ and (b) Ne^+ in the ground state, respectively. The black curves represent the summed total cross sections for ionization and excitation. For He^+ , only the singlet total cross sections are presented for both excitation and ionization. The arrows mark the maximum energies of the returning electron.

is initially in the ground state, a singlet spin state, and that the total spin is preserved during the collision in our nonrelativistic models. The singlet TCSs for $e\text{-He}^+$ collisions are shown in Fig. 4, while only spin-averaged TCSs from prior calculations are currently available for $e\text{-Ne}^+$ collisions. However, due to the uncertainty of the laser intensity distributions in the gas cell and the steep variation of the NSDI yields with peak laser intensity, it is not expected that the sensitivity of the comparison with theory is large enough to justify the computational effort needed to (re)generate TCSs for the singlet spin channels only. In the future, if correlated two-dimensional momentum distributions of the two electrons are available experimentally for the 400 nm laser pulses, then such a calculation will be justified. For electron impact excitation of Ne^+ , the TCSs include combined excitations to 12 excited states from $2s2p^6$ to $2s^22p^45f$. Based on the n^{-3} scaling law, the excitations to higher states can safely be neglected.

For the current purpose, the highest laser intensities are $2.8 \times 10^{15} \text{ W/cm}^2$ and $2.0 \times 10^{15} \text{ W/cm}^2$ for He and Ne, respectively. The arrows in Fig. 4 mark the corresponding maximum returning electron energies of 127 eV and 96 eV, respectively. The figure shows that the sum of the singlet TCSs for He is about half of the spin-averaged one for Ne, although the individual TCSs for He were already increased by about a factor of 2 when the spin conservation was accounted for [15, 36]. For the energy

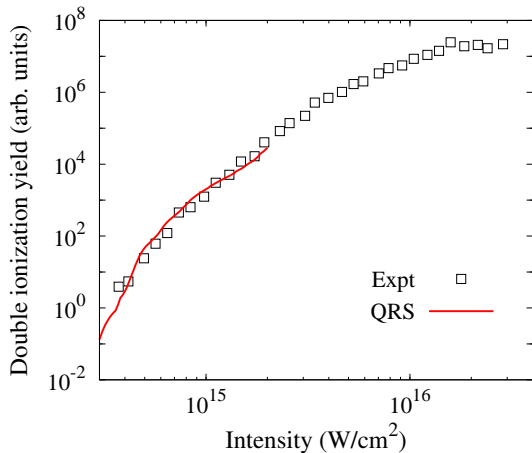


FIG. 5: Double ionization yields for Ne exposed to linearly polarized laser pulses at 400 nm. The experimental data are taken from Ekanayake *et al.* [35], and the simulated results from the QRS model are normalized for good visual agreement with experiment. The calculations include the integration over the focal volume of the laser.

range considered here, excitation dominates ionization for both He^+ and Ne^+ .

With the obtained RWPs and TCSs, the calculation for the total yield of NSDI is straightforward by performing the integration in Eq. (28), in which both the focal-volume averaging and the change of the thresholds due to the presence of the electric field at the time of rescattering are taken into account. The simulated NSDI yields for Ne are plotted as a function of intensity in Fig. 5. Recall that, to fit the experimental measurements of Ekanayake *et al.* [35], a normalization factor is used in Fig. 2. After normalization, similar to the total single ionization rate shown in Fig. 2, the normalized numerical results for NSDI of Ne are again in good accord with experiment.

Experimentally, absolute single-ionization or double-ionization yields can currently not be accurately determined. However, the ratio of double to single ionization from a given experiment can be more definitely obtained. In theoretical calculations, strong-field double and single ionization can be calculated by solving the many-electron TDSE directly. However, such calculations are extremely difficult for Ti-Sapphire and mid-infrared wavelength lasers even for the two-electron helium target. By going to about 400 nm lasers, converged TDSE calculations appear possible. It would be computationally expensive, however, to account for the volume integration, since the latter requires the calculations be carried out over many intensities. Thus it is desirable to develop theoretical models for single and double ionization, by which absolute yields can be calculated accurately, while the ratios of double to single ionization can be compared directly to experiments. The calculations should also be relatively fast, so that volume integration

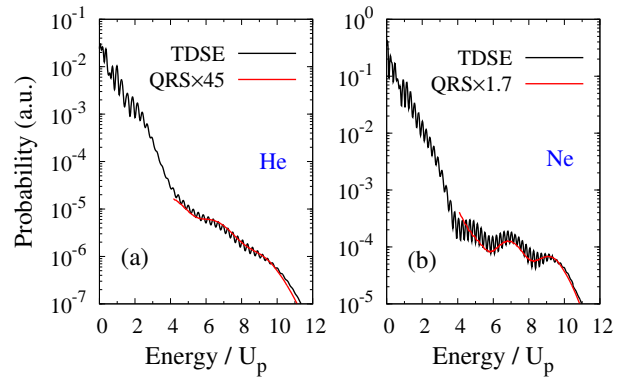


FIG. 6: Comparison of energy spectra between the QRS and TDSE calculations for high-order above-threshold ionization of (a) He exposed to a 390 nm laser pulse at a peak intensity of 8.0×10^{14} W/cm², and (b) Ne exposed to a 400 nm laser pulse at a peak intensity of 9.6×10^{14} W/cm², respectively. All calculations were performed for 5-cycle pulses at a single intensity without focal-volume integration.

can be accounted for.

For single ionization in strong fields, TDSE calculations within the single electron model as described in Section II.B can be readily calculated. Single ionization can also be calculated using the SFA1 model. Even though SFA1 does not give accurate absolute ionization probabilities, it does provide an accurate intensity dependence. By comparing TDSE and SFA1 results, therefore, the normalization factor for single ionization is readily obtained.

To obtain absolute double ionization yields, on the other hand, there are generally no TDSE results available to calibrate a model for any target, and particularly in the nonsequential double-ionization intensity regime. It is well established, however, that in the NSDI intensity regime, double ionization proceeds through electron impact excitation and ionization of the target ion by the returning rescattering electrons. In the QRS theory, the returning electrons are represented by the RWP, which is also responsible for the emission of HATI electrons and HHG. Both HATI and HHG processes are primarily one-electron processes, and hence they can be calculated by solving the one-electron TDSE, as well as by using the SFA2. As explained in Section II.C, however, in SFA2 the cross sections for electron collisions are calculated using the first-order Born approximation. The latter is well known to be inaccurate at lower energies. On the other hand, the RWP is dominated by the intense laser field, once the electron is removed from the parent atom. It has been demonstrated that the RWP has the correct energy dependence and is fairly independent of the target for a given laser pulse. Thus one can obtain the RWP correctly, except for a normalization factor. Within the QRS model, the RWPs for HATI electrons and for NSDI are the same. They differ only by HATI being due to elastic scattering while NSDI is an inelastic scattering

process. The former can be accurately calculated within a one-electron model while the latter requires many-body calculations. According to the QRS theory, both of these calculations are needed for electron scattering without the laser field. Then the RWP can be extracted from SFA2. By replacing the HATI spectrum obtained from the QRS theory with the one calculated by solving the TDSE, the normalization factor can be obtained. In Fig. 6, we compare the high-energy photoelectron spectra from TDSE and QRS. With an appropriately chosen normalization factor, the HATI energy spectra above $4U_p$ due to elastic rescattering of the returning electron with the parent ion, as obtained from the QRS simulations, are in very good agreement with the TDSE results for both He and Ne.

With all the above ingredients carefully prepared, we are finally able to obtain the ratio between double and single ionization. Figure 7 shows the ratio between double and single ionization of He in a 120 fs pulse with a wavelength of 390 nm and Ne in a 40 fs pulse with a wavelength of 400 nm, respectively. In panel 7(a), the measured intensities are multiplied by 1.5, as suggested by Parker *et al.* [20]. With the shift of the measured intensities, the present QRS simulations are in excellent agreement with the experimental data of Sheehy *et al.* [34] as well as with the TDSE calculations of Parker *et al.* [20] for almost the entire intensity range, with the exception being intensities below 5.0×10^{14} W/cm². At these very low intensities, double ionization and the ratios are relatively small. We believe that noise in the experiment and convergence problems in the TDSE calculations are the most likely the reasons for the discrepancies between those results and the QRS predictions. The calculations of van der Hart and Burnett [32] are also based on their version of the rescattering model. Their predicted ratios exhibit a similar intensity dependence but are shifted to higher intensities.

In Fig. 7(b), the experimental data for the double-to-single ionization ratio of Ne were deduced from the total ionization yields of Ne²⁺ and Ne⁺ measured by Ekanayake *et al.* [35]. Again, the QRS simulations are in very good agreement with experiment. The good agreement owes much to the use of accurate electron impact excitation and ionization cross sections calculated with the BSR method. With 400 nm lasers, the returning electron energies are relatively small, and hence thus many-body calculations are essential. In the actual numerical calculations, shorter laser pulses (65 fs for He and 40 fs for Ne, respectively) than those in the experiments were used, since the ratios of the total ionization yields are not expected to depend significantly on the duration of the laser pulses.

It is interesting to note from Fig. 7 that the intensity dependence of the measured double-to-single ionization ratio of He is rather different from that of Ne. While the ratio for He changes by approximately a factor of 200 over the measured intensity range, the ratio for Ne only changes by a factor of less than 35. The larger ratio for

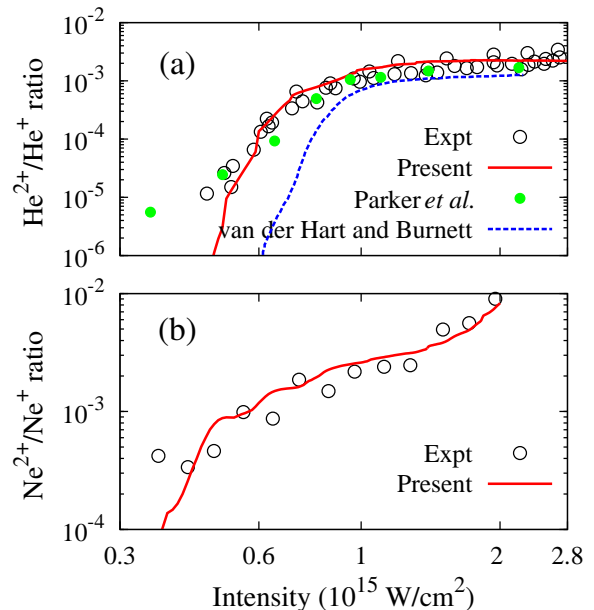


FIG. 7: Ratio between double and single ionization as a function of intensity for (a) He in a 120 fs pulse with a wavelength of 390 nm, and (b) Ne in a 40 fs pulse with a wavelength of 400 nm. In (a), the present simulations are compared with the experimental data of Sheehy *et al.* [34], the TDSE calculations of Parker *et al.* [20], and the calculations of van der Hart and Burnett [32] based on the rescattering model. All experimental data points were shifted to higher intensity by 50%, as suggested by Parker *et al.* [20]. In (b), the present results are compared with the experimental data of Ekanayake *et al.* [35].

Ne is due to the larger returning electron wave packets for Ne in the same intensity range when compared to He. Figure 4 shows that the excitation and ionization cross sections between Ne⁺ and He⁺ differ by about a factor of two, but Fig. 6 shows that the probability density for HATI electrons at the same electron energy is one to two orders larger for Ne when compared to He.

IV. CONCLUSIONS

Using the QRS model, we have performed numerical simulations for the double to single ionization ratios of He and Ne exposed to laser pulses at 390 nm and 400 nm, respectively. Since the returning electron wave packet is usually obtained from the strong-field approximation (SFA2), an overall normalization factor has to be determined. According to the rescattering model, the returning electron wave packets for HATI electrons and for NSDI processes are the same, and hence the correct returning electron wave packet can be extracted from solving the TDSE for HATI electrons using the one-electron model. By comparing the returning electron wave packets obtained from TDSE and SFA2, an over-

all renormalization factor is obtained. Once this factor is determined, the QRS theory can be applied to NSDI processes using accurate electron impact excitation and ionization cross sections from method such as BSR, where many-electron effects are properly accounted for. Taking advantage of the simplicity of the QRS theory, single and double ionization yields can be calculated by including the intensity distributions of the focused laser beam. The resulting ratios calculated with these procedures are then compared to experimental data. The present results were found to be in very good agreement with experiment for both He and Ne, thereby validating the QRS model for calculating nonsequential double ionization, provided that accurate electron impact excitation and ionization cross sections are available.

V. ACKNOWLEDGMENT

This work was supported by the National Natural Science Foundation of China under Grant No. 11274219, the

STU Scientific Research Foundation for Talents, and the Scientific Research Foundation for the Returned Overseas Chinese Scholars, State Education Ministry. O.Z. and K.B. were supported by the U.S. National Science Foundation under Grants No. PHY-1430245 and No. PHY-1520970, as well as the XSEDE Allocation No. PHY-090031. C.D.L. was supported, in part, by the Chemical Sciences, Geosciences and Biosciences Division, Office of Basic Energy Sciences, Office of Science, U.S. Department of Energy, under grant number DE-FG02-86ER13491.

-
- [1] J. L. Krause, K. J. Schafer, and K. C. Kulander, *Phys. Rev. Lett.* **68**, 3535 (1992).
 - [2] P. B. Corkum, *Phys. Rev. Lett.* **71**, 1994 (1993).
 - [3] B. Yang, K. J. Schafer, B. Walker, K. C. Kulander, P. Agostini, and L. F. DiMauro, *Phys. Rev. Lett.* **71**, 3770 (1993); G. G. Paulus, W. Nicklich, H. Xu, P. Lambropoulos, and H. Walther, *Phys. Rev. Lett.* **72**, 2851 (1994).
 - [4] F. Krausz and M. Ivanov, *Rev. Mod. Phys.* **81**, 163 (2009).
 - [5] A. L’Huillier, L. A. Lompre, G. Mainfray, and C. Manus, *Phys. Rev. Lett.* **48**, 1814 (1982); *Phys. Rev. A* **27**, 2503 (1983).
 - [6] D. N. Fittinghoff, P. R. Bolton, B. Chang, and K. C. Kulander *Phys. Rev. Lett.* **69**, 2642 (1992).
 - [7] C. D. Lin, A.-T. Le, Z. Chen, T. Morishita, and R. Lucchese, *J. Phys. B* **43**, 122001 (2010).
 - [8] Z. Chen, A.-T. Le, T. Morishita, and C. D. Lin, *Phys. Rev. A* **79**, 033409 (2009).
 - [9] Z. Chen, A.-T. Le, T. Morishita, and C. D. Lin, *J. Phys. B* **42**, 061001 (2009).
 - [10] Y. Liang, *Phys. Rev. A* **82**, 055403 (2010).
 - [11] Z. Chen, J. Ye, Y. Xu, *Chin. Phys. B* **24**, 103203 (2015).
 - [12] A.-T. Le, R. R. Lucchese, S. Tonzani, T. Morishita, and C. D. Lin, *Phys. Rev. A* **80**, 013401 (2009).
 - [13] A.-T. Le, H. Wei, C. Jin, and C. D. Lin, *J. Phys. B* **49**, 053001 (2016).
 - [14] S. Micheau, Z. Chen, A.-T. Le, and C. D. Lin, *Phys. Rev. A* **79**, 013417 (2009).
 - [15] Z. Chen, Y. Zheng, W. Yang, X. Song, J. Xu, L. F. DiMauro, O. Zatsarinny, K. Bartschat, T. Morishita, S. F. Zhao, and C. D. Lin, *Phys. Rev. A* **92**, 063427 (2015).
 - [16] Z. Chen, Y. Liang, and C. D. Lin, *Phys. Rev. Lett.* **104**, 253201 (2010); *Phys. Rev. A* **82**, 063417 (2010).
 - [17] Z. Chen, Y. Liang, D. H. Madison, and C. D. Lin, *Phys. Rev. A* **84**, 023414 (2011).
 - [18] A. M. Perelomov, V. S. Popov, and M. V. Terent’ev, *Sov. Phys. JETP* **24**, 207 (1967).
 - [19] S.-F. Zhao, A.-T. Le, C. Jin, X. Wang, and C. D. Lin, *Phys. Rev. A* **93**, 023413 (2016).
 - [20] J. S. Parker, L. R. Moore, D. Dundas, and K. T. Taylor, *J. Phys. B* **33**, L691 (2000).
 - [21] O. Zatsarinny, *Comp. Phys. Commun.* **174**, 173 (2006).
 - [22] O. Zatsarinny and K. Bartschat, *J. Phys. B* **46**, 112001 (2013).
 - [23] M. V. Ammosov, N. B. Delone, and V. P. Krainov, *Zh. Eksp. Teor. Fiz.* **91**, 2008 (1986).
 - [24] X. M. Tong and C. D. Lin, *J. Phys. B* **38**, 2593 (2005).
 - [25] M. Lewenstein, K. C. Kulander, K. J. Schafer, and P. H. Bucksbaum, *Phys. Rev. A* **51**, 1495 (1995).
 - [26] X. M. Tong and C. D. Lin, *J. Phys. B* **38**, 2593 (2005).
 - [27] X. M. Tong and S.-I. Chu, *Chem. Phys.* **217**, 119 (1997).
 - [28] T. Morishita, Z. Chen, S. Watanabe and C. D. Lin, *Phys. Rev. A* **75**, 023407 (2007).
 - [29] D. O. Harris, G. G. Engerholm and W. D. Gwinn, *J. Chem. Phys.* **43**, 1515 (1965).
 - [30] A. S. Dickinson and P. R. Certain, *J. Chem. Phys.* **49**, 4209 (1968).
 - [31] J. C. Light and R. B. Walker, *J. Chem. Phys.* **65**, 4272 (1976).
 - [32] H. W. van der Hart and K. Burnett, *Phys. Rev. A* **62**, 013407 (2000).
 - [33] E. Eremina, X. Liu, H. Rottke, W. Sandner, A. Dreischuh, F. Lindner, F. Grasbon, G. G. Paulus, H. Walther, R. Moshhammer, B. Feuerstein, and J. Ullrich, *J. Phys. B* **36**, 3269 (2003).
 - [34] B. Sheehy, R. Lafon, M. Widmer, B. Walker, L. F. DiMauro, P. A. Agostini, and K. C. Kulander, *Phys. Rev. A* **58**, 3942 (1998).
 - [35] N. Ekanayake, S. Luo, B. L. Wen, L. E. Howard, S. J. Wells, M. Videtto, C. Mancuso, T. Stanev, Z. Condon, S. LeMar, A. D. Camilo, R. Toth, W. B. Crosby, P. D. Grugan, M. F. Decamp, and B. C. Walker, *Phys. Rev. A*

86, 043402 (2012).

[36] Hugo W. van der Hart, J. Phys. B **33**, L699 (2000).